Very Long Baseline Interferometry and the VLBA
ASP Conference Series, Vol. 82, 1995
J. A. Zensus, P. J. Diamond, and P. J. Napier (eds.)

Printed June 13, 1995

CHAPTER 9

An Introduction to Calibration Techniques for VLBI

JAMES M. MORAN

HARVARD-SMITHSONIAN CENTER FOR ASTROPHYSICS

VIVEK DHAWAN

NATIONAL RADIO ASTRONOMY OBSERVATORY

Abstract This chapter discusses the various techniques used to calibrate the amplitude and phase of VLBI data. The effect of residual calibration errors on image quality is also considered.

Contents

9.1 Introduction

This chapter describes the basic physical and statistical problems encountered in the process of calibrating VLBI data. The purpose of this chapter is to acquaint the reader with the fundamental issues rather than set forth an encyclopedic or cookbook approach to calibration. The need for calibration and the limitations of self-calibration procedures are presented. The four types of calibration: delay, fringe rate, amplitude and phase are described. The amplitude calibration is affected primarily by aperture efficiency, atmospheric absorption and pointing errors. Direct phase calibration has rarely been possible up to now. However, the processes that effect the coherent integration time such as phase noise in the frequency standards and path length fluctuations in the atmosphere are important in data processing. The use of phased arrays as VLBI elements are explained. Finally the recognition of calibration errors in image defects is described.

The fundamental task of calibration can be stated quite succinctly. One hopes to estimate a set of fringe visibilities V_{ij} between the antennas i and j, but because of various instrumental problems one actually measures quantities V'_{ij}. Many effects depend on the antennas alone and can be described by the equation

$$V'_{ij} = G_i G_j^* V_{ij} \;, \tag{9.1}$$

where G_i and G_j are complex gain factors that characterize the instrumental amplitude and phase errors at each antenna. For example, if a cloud drifts through the beam of antenna i and introduces a phase shift of $\pi/2$ during a measurement, its effect is characterized as a complex gain of $G_i = e^{i\frac{\pi}{2}}$ for that time. There are other effects that are baseline dependent and are more difficult to deal with. Baseline dependent gain coefficients, i.e., G_{ij}, cannot be factored into station dependent gains as in equation 9.1.

The need for detailed discussion of calibration procedures could be questioned. Why not draw on the years of experience with the VLA and other connected element interferometers where the calibration relies on the procedure of interleaving observation of the program source with those on an unresolved calibrator source that is nearby in angle? Such observations directly provide the quantities $G_i G_j^*$ and equation 9.1 can be inverted to obtain the desired V_{ij}s. The fundamental problem of adapting such a scheme to VLBI data is that there are few unresolved sources at the angular scale of milliarcseconds, so calibration sources are generally far removed from program sources. Hence, such quantities as the atmospheric phase shift and the elevation dependent collecting area of the antennas will differ. In addition, VLBI has a broader range of instrumental problems. For example, the clocks at the stations may not be running synchronously.

A second objection might be that calibration should be unimportant because of the very powerful techniques of self-calibration or hybrid mapping that rely on closure relations that remove or mitigate the effect of complex gain errors. We briefly describe these relations, which are graphically shown in figure 9.1. Suppose we have three stations, with instrumental phase errors ϕ_1, ϕ_2, and ϕ_3, which contribute gain factors $e^{i\phi_1}$, $e^{i\phi_2}$, and $e^{i\phi_3}$. We could correct them if we

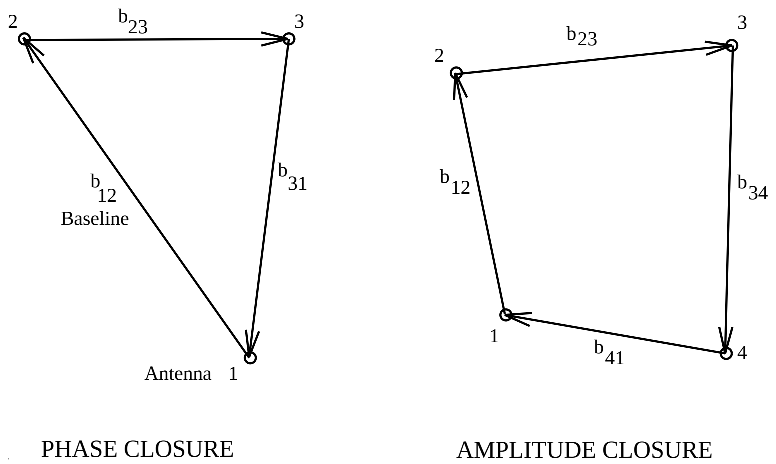

Figure 9.1: *Left:* A set of three baselines in an array that forms a triangle, which can be used to generate a phase closure variable. *Right:* A set of four baselines that forms a quadrangle, which can be used to generate an amplitude closure variable.

knew what they were. The visibility phases on the three baselines will be

$$\begin{aligned} \phi_{12} &= \mathbf{b}_{12}\cdot\mathbf{s} + \psi_{12} + \phi_1 - \phi_2 \\ \phi_{23} &= \mathbf{b}_{23}\cdot\mathbf{s} + \psi_{23} + \phi_2 - \phi_3 \\ \phi_{31} &= \mathbf{b}_{31}\cdot\mathbf{s} + \psi_{31} + \phi_3 - \phi_1, \end{aligned} \tag{9.2}$$

where $\mathbf{b}_{ij}$ is the baseline vector between stations i and j, $\mathbf{s}$ is the unit vector in the direction of the source, ψ_{ij} is the phase of the fringe visibility with respect to the field center defined by $\mathbf{s}$. The sum of the phases around this triangle is

$$\Phi_{123} = \phi_{12} + \phi_{23} + \phi_{31} = \psi_{12} + \psi_{23} + \psi_{31}\,. \tag{9.3}$$

The baseline terms cancel because the baselines, when factored out of the dot product, form a closed triangle ($\mathbf{b}_{12} + \mathbf{b}_{23} + \mathbf{b}_{31} = 0$) . Baseline errors and source position errors cancel. Hence Φ is free of instrumental effects and geometric errors and can be used to determine the source structure (contained in the ψ_{ij} terms). Note that if the source is a point source then Φ_{123} is 0. The amplitude closure conditions apply to four baselines that form a closed quadrangle, and is defined as

$$Q = \frac{|V'_{12}||V'_{34}|}{|V'_{23}||V'_{41}|} = \frac{g_1 g_2 |V_{12}| g_3 g_4 |V_{34}|}{g_2 g_3 |V_{23}| g_4 g_1 |V_{41}|} = \frac{|V_{12}||V_{34}|}{|V_{23}||V_{41}|}\,, \tag{9.4}$$

where the g_is are the magnitudes of the respective gains, G_is. The closure amplitudes can be used most effectively in the high signal-to-noise regime with large arrays. The closure conditions require that fringes have been detected on each

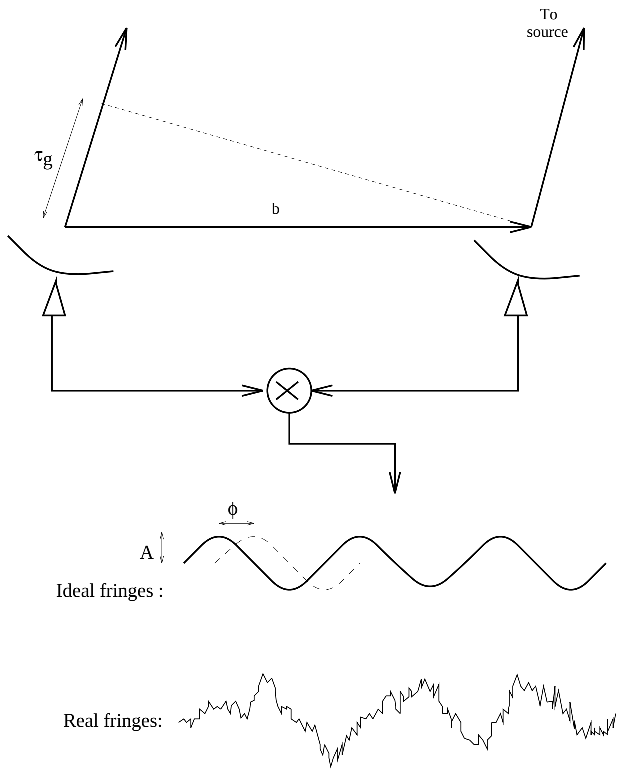

Figure 9.2: Simplified diagram of an interferometer with "ideal" fringes and "real" fringes degraded by receiver noise and atmospheric effects. Some critical elements of the system, e.g., frequency standards, mixers, and tape recorders, are not shown.

baseline separately. For the VLBA, the minimum detectable signal is about 25 mJy. The fraction of the phase and amplitude information that can be recovered is $N-2/N$ and $(N-3)/(N-1)$, respectively. The use of phase and amplitude closure information in image restoration procedures is discussed extensively by Pearson and Readhead (1984). Self-calibration has several limitations. For small arrays a significant fraction of the phase and amplitude information cannot be recovered. Also, as is clear from equations 9.3 and 9.4, the information about the total flux density and also the absolute position of the source are lost.

A cartoon of an interferometer fringe pattern is shown in figure 9.2, with a case of no noise and one with noise and other sources of errors. In the following sections we discuss the basic physics behind these errors. Later chapters in this book describe these effects in more detail and give a more step-by-step approach to calibration implementation. Much of the information can be found in Thompson, Moran and Swenson (1986, hereinafter TMS), Moran (1989), and Rogers (1993a).

9.2 Delay Calibration

The signals received at the interferometer elements must be aligned properly or else the fringe amplitude will suffer degradation. This effect can be understood in terms of one of the fundamental theorems of Fourier Transform analysis, the shift theorem. If a function $f(t)$ has transform $F(\omega)$, then $f(t-\tau_e)$ has transform $F(\omega)\exp(i\omega\tau_e)$. These transform pairs can be written

$$f(t) \leftrightarrow F(\omega) \tag{9.5}$$

and

$$f(t-\tau_e) \leftrightarrow F(\omega)\, e^{i\omega\tau_e}\,. \tag{9.6}$$

In particular, if a correlation function $R(\tau)$ at a point in the (u,v) plane has a transform $V(\omega)$, then $R(\tau-\tau_e)$ transforms into a visibility function given by

$$R(\tau-\tau_e,u,v) \leftrightarrow V(\omega,u,v)\, e^{i\omega\tau_e}\,. \tag{9.7}$$

Thus a delay error causes a phase shift with frequency. If the frequency interval is $\Delta\nu$ (the bandwidth in the case of continuum analysis or the spectral resolution in the case of spectral line analysis) then the averaging of the function $e^{iw\tau_e}$ in equation 9.7 over frequency $\Delta\nu$ gives a reduction in amplitude of

$$|G_{12}| = \frac{\sin \pi\Delta\nu\tau_e}{\pi\Delta\nu\tau_e}\,. \tag{9.8}$$

Note that this is a baseline dependent error, as opposed to a station dependent error since it depends on the relative delay error between the two antennas and cannot be factored into the form $G_1G_2^*$. Note however that clock offsets do close. The delay error due to station clock errors can be readily determined by observations of a calibrator source. The accuracy of a delay measurement is (e.g., TMS)

$$\Delta\tau \sim \frac{1}{2\Delta\nu}\frac{1}{SNR}\,, \tag{9.9}$$

where $\Delta\nu$ is the total bandwidth, $1/2\Delta\nu$ is the Nyquist sampling rate, and SNR is the signal-to-noise ratio of the measurement.

9.3 Fringe-Rate Calibration

The frequency standards that control the station clocks may not be exactly set to the desired frequency, which makes the delay error change linearly with time and also introduces an instrumental phase that changes linearly with time. Hence

$$\tau_e = \tau_{e_o} + \left(\frac{\delta\nu}{\nu}\right) t\,, \tag{9.10}$$

where $\delta\nu/\nu$ is the fractional frequency offset of the time standard. The gain factor will have a term of the form $G_i = e^{[i2\pi(\delta\nu/\nu)]\nu t}$. If the integration period T is significant with respect to $(\delta\nu/\nu)^{-1}$ then visibility amplitude will decrease by the amount

$$G_{12} = \frac{\sin\pi\left(\frac{\delta\nu}{\nu}\right)\nu T}{\pi\left(\frac{\delta\nu}{\nu}\right)\nu T}\,, \tag{9.11}$$

where $\delta\nu/\nu$ is here the difference in fractional frequencies between the standards at the stations. The frequency offsets of the frequency standards can be determined either by measuring τ_e at several epochs or by measuring the fringe rate offset.

In VLBI the determination of the station clocks and frequency offsets has often been a formidable task known as "finding the fringes." With an array such as the VLBA, which will operate continuously, these parameters will be closely monitored.

Astrometric VLBI measurements have been made almost exclusively with delay or fringe rate variables. Phase has generally been too difficult to calibrate, but differential astrometry has been done with phase information on closely spaced continuum sources and maser clusters. Astrometry on continuum sources is usually based on broad band delay measurements whereas astrometry on spectral line sources, which are inherently narrow-band, is usually performed on fringe rate measurements. Final calibration parameters are modeled and determined during the least-mean-squares data analysis that yields the desired source positions.

9.4 Amplitude Calibration

9.4.1 Antenna Calibration

The power received by a radio telescope is given by, e.g., Rolfs (1986)

$$P = \frac{1}{2}\Delta\nu\int I_\nu\left(\Omega\right)A\left(\Omega\right)d\Omega\,, \tag{9.12}$$

where I_ν is the specific intensity of the source as a function of angle Ω, A is the effective collecting area of the antenna and $\Delta\nu$ is the receiver bandwidth. By the Nyquist theorem (which is the one dimensional blackbody relation), the received power can be related to an equivalent antenna temperature T_A by the relation, $P = kT_A\Delta\nu$, where k is Boltzmann's constant. If the source is small with respect to the antenna beam, the usual case in VLBI, then A can be taken out of the integral as a constant. The integral of intensity is the flux density S so that

$$T_A = \frac{SA}{2k}\,. \tag{9.13}$$

For a VLBI system based on a quantized signal representation, the computed correlation function ρ, or in the case of spectral line data, the cross power spectrum $\rho(\omega)$, is converted to temperature units by multiplication by the geometric mean of the system temperatures, T_{s_1} and T_{s_2}. As suggested by equation 9.13, the conversion to units of flux density is accomplished by multiplying by $2k/\sqrt{A_1 A_2}$. Hence the relation between visibility and normalized correlation (ignoring digital processing factors) is

$$V_{12} = \rho \cdot 2k \cdot 10^{26} \left[\frac{T_{s_1} T_{s_2}}{A_1 A_2} \right]^{1/2} [\mathrm{Jy}] \,, \tag{9.14}$$

where the areas are in m^2 and k is in w K^{-1}.

The rms sensitivity is proportioned to the term in brackets. Thus a useful quantity in describing the performance of a station is the system temperature in units of Janskys, T'_{s_i}, or the system equivalent flux density (SEFD), which is given by

$$T'_{s_i} = \frac{2760\, T_{s_i}}{A_i} \,, \tag{9.15}$$

where A_i, is the effective collecting area in square meters. Then the normalization is simply $V_{12} = \rho \sqrt{T'_{s1} T'_{s2}}$. Note that in the estimate of V any errors in the amplitude of the temperature reference of the radiometer (eg., noise tube or thermal load) cancel in the estimate of T'_{s_i}. That is, if the temperature reference is overestimated by 10% then both the system temperature and the collecting area will be overestimated by 10%, and T'_S will be unaffected.

The ratio of the effective collecting area of the antenna to the geometric area is the aperture efficiency, η_A. A typical parabolic reflector antenna may have the following components of efficiency

$$\eta_A = \eta_R \eta_T \eta_{SO} \eta_B \eta_S \,, \tag{9.16}$$

whose definitions and representative values are:

$\eta_R =$	radiation efficiency	$= 0.96$
$\eta_T =$	taper illumination	$= 0.90$
$\eta_{SO} =$	spillover	$= 0.95$
$\eta_B =$	feed leg and subreflector blockage	$= 0.90$
$\eta_S =$	surface accuracy	$= 0.90$
$\eta_A =$		0.66 .

Consider the surface accuracy term, η_S. We can think of the surface of the reflector as consisting of many segments with deviations from a perfect parabola given by ϵ, which is a gaussian random variable, with probability distribution

$$p(\epsilon) = \frac{1}{\sqrt{2\pi}\sigma} e^{-\frac{\epsilon^2}{2\sigma^2}} \,, \tag{9.17}$$

where $\langle\epsilon\rangle = 0$ and $\langle\epsilon^2\rangle = \sigma^2$. A very important relation, which can be proved by direct calculation from equation 9.17 is

$$\langle e^{i\epsilon}\rangle = \langle\cos\epsilon + i\sin\epsilon\rangle = \langle\cos\epsilon\rangle = \int_{-\infty}^{\infty}\cos\epsilon\; p(\epsilon)\,d\epsilon = e^{-\frac{\sigma^2}{2}}\,. \tag{9.18}$$

A surface deviation of ϵ causes a phase shift in the electric field of $\psi \sim 4\pi\epsilon/\lambda$, where λ is the wavelength (the extra factor of two comes from the reflection), as long as the f/d ratio of the antenna is large, and hence the electric field components at the focus of the antenna have a gaussian random phase distribution with $\sigma_\psi = 4\pi\sigma/\lambda$. If we suppose that the antenna has N independent panels then the collecting area is proportional to the square of the electric field, or

$$A = A_g\left\langle\left|\frac{1}{N}\sum e^{i\psi_i}\right|^2\right\rangle, \tag{9.19}$$

where A_g is the geometric area of the antenna ($\pi d^2/4$, where d is the diameter of the antenna). If $\sigma_\psi = 0$, then all the phase factors are unity and $A = A_g$. Expressing equation 9.19 as a double summation gives

$$A = \frac{A_g}{N^2}\sum_{i,j}\left\langle e^{i(\psi_i-\psi_j)}\right\rangle \simeq A_g\langle e^{i\psi_i}\rangle^2, \tag{9.20}$$

where we ignored the terms where $i = j$. From equations 9.18 and 9.20 we obtain

$$A = A_g e^{-\left(\frac{4\pi\sigma}{\lambda}\right)^2}\,. \tag{9.21}$$

This equation is known in radio astronomy as the Ruze formula and in other branches of astronomy as the Strehl ratio . An antenna with $\sigma/\lambda = 1/20$, a standard measure, gives $\eta_S = 0.67$.

As an antenna with an alt-azimuth mount is moved in elevation, the reflector distorts, changing the way in which the electric field components combine at the feed. Hence the effective collecting area is a function of elevation angle. In practice, the subreflector is moved as a function of elevation to compensate for the change in position of the focus. Most antennas are set to have maximum efficiency at an elevation of $\sim 45°$. The so-called "gain curve" of an antenna is a plot of effective collecting area in units of K/Jy or from equation 9.15, $A/2760$ as a function of elevation angle. Examples of gain curves are shown in figure 9.3. Note that the formal definition of antenna gain is $4\pi A/\lambda^2$. This is the gain relative to an isotropic radiator.

9.4.2 Atmospheric Opacity

The absorption of radio waves in the atmosphere at microwave and millimeter frequencies is due primarily to spectral line transitions of water vapor and oxygen.

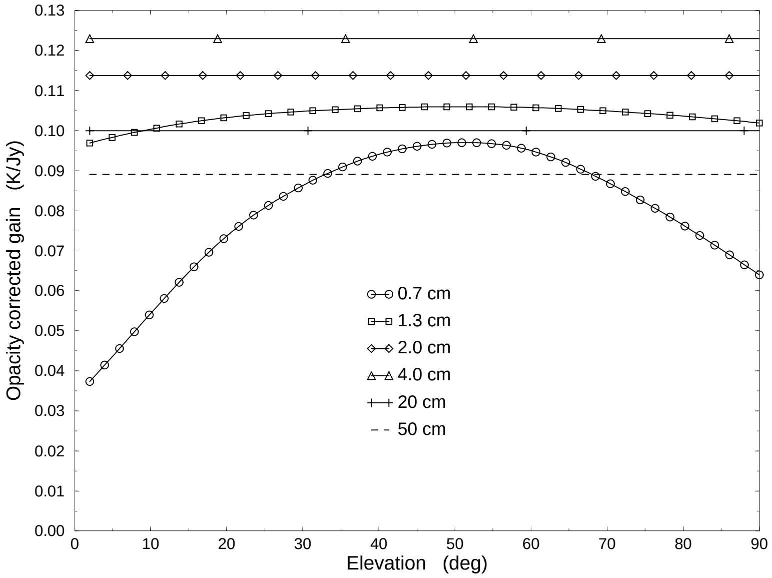

Figure 9.3: The opacity corrected gain curves for the VLBA antenna at Fort Davis, TX, at the wavelengths indicated.

The absorption as a function of frequency is shown in figure 9.4. For most purposes we can assume that the atmosphere is a plane parallel layer of absorbing gas above the antenna, which has temperature T_o and zenith opacity τ_0 at the observing frequency. The path length through the atmosphere is approximately proportional to $\sec z$ where z is the local zenith angle, and the total opacity is $\tau = \tau_0 \sec z$. Hence, the system temperature will consist of the receiver temperature, T_R, plus a contribution due to the atmosphere and (from the usual solution of the equation of radiative transfer) can be written as

$$T_S = T_R + T_0\left(1 - e^{-\tau_0 \sec z}\right) . \tag{9.22}$$

$$T_S \simeq T_R + T_0 \tau_0 \sec z . \tag{9.23}$$

Measurements of T_S are acquired as a function of z and plotted as a function of $\sec z$ (see figure 9.5). The slope of a straight line fit to this data is $T_0\tau_0$ and the extrapolated intercept at $\sec z = 0$ (no atmosphere) is T_R (86 K for the case shown in fig. 9.5). The opacity τ_0 can be estimated by use of the surface temperature for T_0. Note that at large values of $\sec z$ the functional dependence of T_S will become non linear (i.e., it will saturate) because the plane parallel atmosphere assumption breaks down and because of the non-linearity of the exponential term in equation 9.22 when $(\tau_0 \sec z) > 1$. Of course the opacity can be determined from the full tipping scan by use of a non-linear least squares

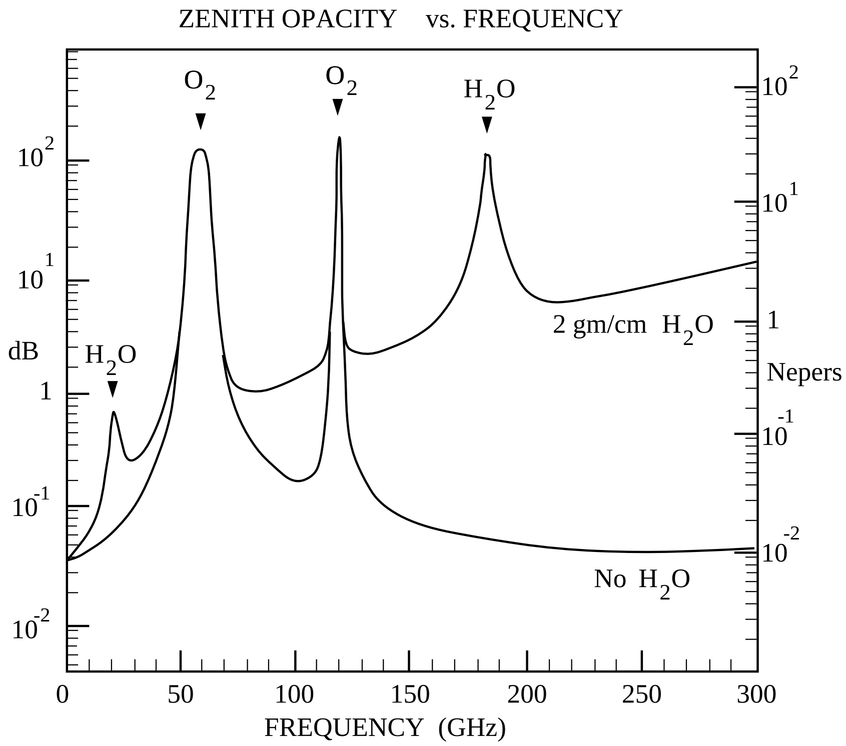

Figure 9.4: The zenith atmospheric opacity versus frequency for two different amounts of water vapor (from TMS).

algorithm (Leppänen 1993). Ground pickup due to spillover can vary as a function of zenith angle and lead to errors in the estimation of τ_0.

In modern receivers T_R is nearly constant over long periods of time. In this case any individual measurement of T_S at a given time and elevation angle can be converted into an opacity, that is

$$\tau = -\ln\left[\frac{T_0 + T_R - T_S}{T_0}\right] . \tag{9.24}$$

The gain curve of an antenna can be measured after the opacity has been estimated by tracking a calibration source through a range of zenith angles since

$$T_A(z) = \frac{SA(z)}{2k} e^{-\tau_0 \sec z} , \tag{9.25}$$

which can be solved for $A(z)$. Note that changes in the collecting area don't effect the tipping scan measurements because the atmosphere fills the antenna beam.

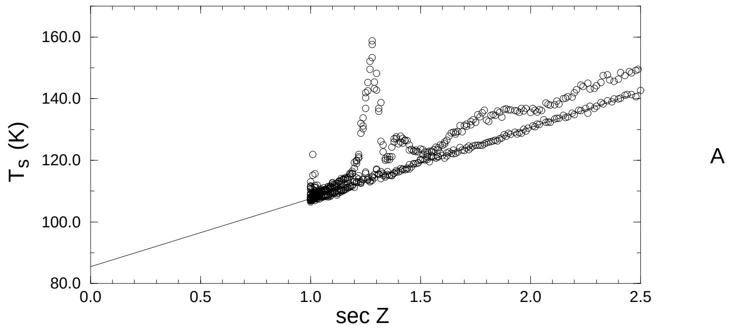

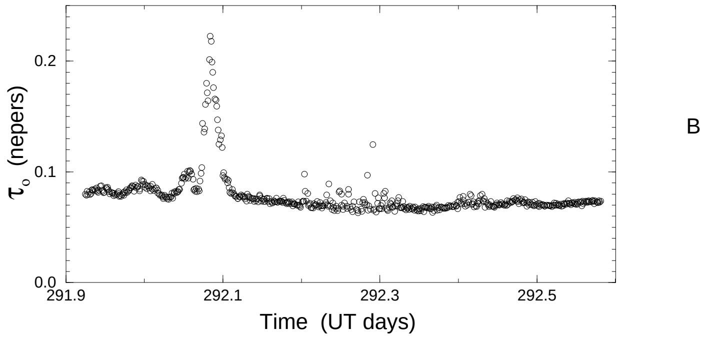

Figure 9.5: *Top:* A plot of system temperature versus $\sec z$ which can be used to determine the receiver temperature and atmospheric opacity *(Bottom)*. The two tracks show the source rising and setting. The system temperature is approximately a linear function of $\sec z$ (see equation 9.23). Deviations from the straight line can be interpreted as fluctuations in opacity, τ_0, as shown in B.

It is common practice to refer the system temperature to a point above the atmosphere by dividing T_S by $\exp(-\tau_0 \sec z)$. This modified system temperature T_S^* is given by

$$T_S^* = T_R e^{\tau_0 \sec z} + T_0 \left(e^{\tau_0 \sec z} - 1\right) . \tag{9.26}$$

T_S^* incorporates the two effects of additive atmospheric noise and signal attenuation. Hence the use of T_S^* in equation 9.15 will correct for both system temperature and atmospheric absorption effects. An example of the gain factors for an array are shown in figure 9.6.

The effective collecting area can also change if there are antenna pointing errors. These errors are often significant in VLBI where antennas are used at frequencies above their initially planned limit. Suppose that the gain or collecting area of a telescope is a gaussian function with full-width-at-half-maximum

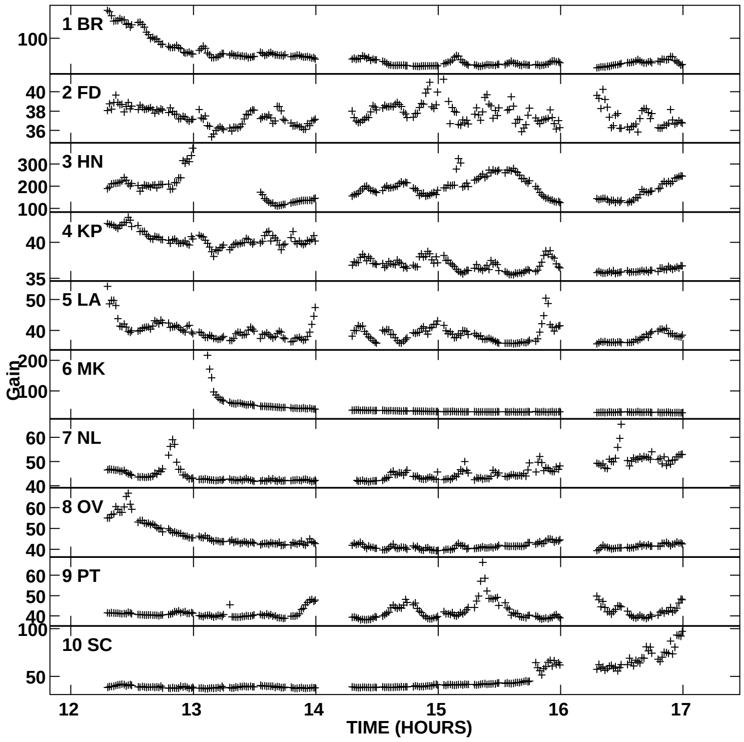

Figure 9.6: The gain factors of 5 antennas of the VLBA at 43 GHz for a 6 hour experiment. These gain factors correct for variations in collecting area, system temperature, and atmospheric opacity.

w, which is approximately $1.2\lambda/d$, and that the pointing error in each axis is described as an independent gaussian random variable with rms deviation in each axis of σ_p. It is easy to show that the expectation of the effective collecting area is given by

$$\langle A \rangle = \eta_A A_g \left[\frac{1}{1+r^2} \right] , \tag{9.27}$$

where $r = \left(\sqrt{8 \ln 2}\right) \sigma_p / \mathrm{w}$, and that the fractional rms deviation is

$$\frac{\sigma_A}{\langle A \rangle} = \frac{r^2}{\sqrt{1+2r^2}} . \tag{9.28}$$

Various values of $\langle A \rangle / \eta_A A_g$ and $\sigma_A / \langle A \rangle$ are listed in table 9.1. Hence, an antenna with an rms pointing error of 10% of its beamwidth in each axis will suffer a mean loss of 5% in collecting area and the collecting area will vary by $\pm 5\%$. Pointing

Table 9.1: Gain reduction due to pointing errors

$\frac{\sigma_p}{w}$	r	$\langle A\rangle/\eta_A A_g$	$\sigma_A/\langle A\rangle$
0	0	1	0
0.1	0.23	0.95	0.05
0.2	0.47	0.82	0.18
0.3	0.71	0.66	0.36
0.4	0.95	0.53	0.53
0.5	1.18	0.42	0.71

errors can be calibrated to a certain extent if the flux density of a nearby source is frequently monitored. This technique has been used effectively for Sgr A* (Lo et al. 1993). Pointing errors can be corrected in spectral line observations by use of the total power spectra (see chapter 11).

Finally we mention that the full effective areas of the antennas in an array will not be achieved if the polarizations of the antennas are not matched. For example, suppose two stations operate with linear polarization with position angles of α_1 and α_2 on the sky. The visibility will be reduced by

$$G_{12} = |\cos(\alpha_1 - \alpha_2)| \; . \tag{9.29}$$

Needless to say, attempts to observe unpolarized sources are severely thwarted when $\alpha_1 - \alpha_2 = \pi/2$. Many failed VLBI experiments have been traced to this sort of blunder. VLBI observations are usually made in circular polarization in order to eliminate problems caused by the differential parallactic angle of observations and Faraday rotation in the ionosphere.

9.5 Phase Calibration

Direct phase calibration is rarely attempted in VLBI except in cases where a calibration source lies very close to the program source. In maser sources, phase calibration has been particularly useful wherein one maser spectral component in a cluster of masers subtending an area of less than a few arcseconds can be used as a phase reference (see chapter 11). The principal reason to be cognizant of phase errors is to be able to choose an integration time short enough that phase errors do not lead to fringe amplitude reductions. These are quite serious since they are baseline dependent and may not be corrected by the application of the closure relations. All of those matters are extensively discussed in chapter 9 of TMS.

9.6 Coherent and Incoherent Averaging

We begin this section by showing that an estimate of the fringe amplitude can be obtained from a time sequence of fringe visibility measurements if the sample

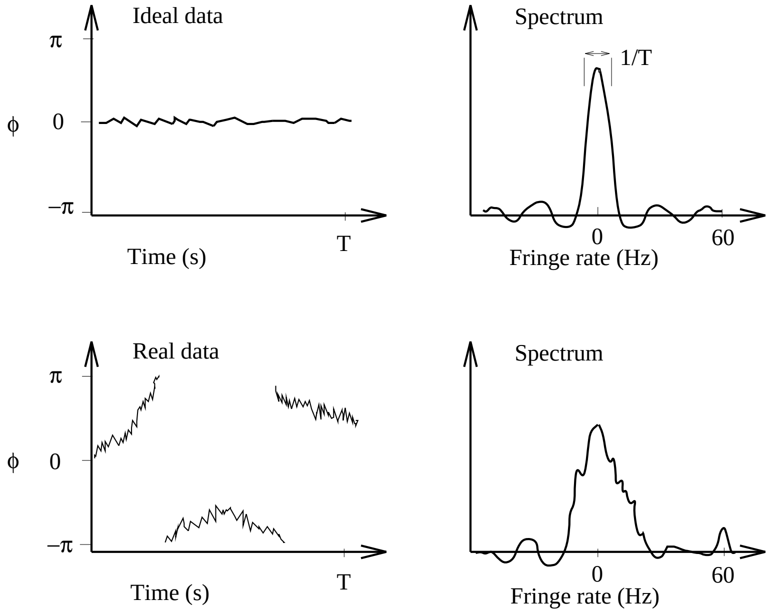

Figure 9.7: *Top left:* Phase versus time for perfect data, i.e., $\phi = 0$. *Top right:* The Fourier transform of $e^{i\phi_i}$ is a sinc function, or with discrete samples at intervals of $1/T$, the normal procedure, a delta function. *Lower left:* A more realistic plot of phase versus time, showing both short term and long term fluctuations. *Lower right:* Fourier transform of the corrupted phase function $e^{i\phi_i}$. Notice the spectral components at 60 Hz, which are commonly seen and are caused by coupling of the local oscillator to the power line.

measurement time is less than the time scale for significant phase fluctuations. Suppose that the fringe visibility, $\mathcal{A}$, is constant but the measured visibility is corrupted by some sort of phase noise process, ϕ_i, that is

$$z_i = \mathcal{A}e^{i\phi_i}\,. \tag{9.30}$$

Neglect for the moment the thermal noise introduced by the receiver. The Fourier transform of the temporal sequence of fringe visibilities is the fringe frequency spectrum, Z_i. For incorrupted data the fringe frequency spectrum is a "delta function" whose amplitude equals the fringe amplitude. In the presence of phase noise, the signal is distributed in the fringe-frequency spectrum as shown in figure 9.7. By Parseval's theorem

$$\sum z_i z_i^* = \frac{1}{N}\sum Z_i Z_i^*\,, \tag{9.31}$$

or, from equation 9.30,

$$\mathcal{A} = \frac{1}{N}\left[\sum Z_i Z_i^*\right]^{1/2}. \tag{9.32}$$

Clark (1968) first applied Parseval's theorem to the problem of estimating fringe amplitude in the presence of phase noise and he showed that if it is necessary to reduce the sample integration time to the reciprocal of the bandwidth, $\Delta\nu^{-1}$, then the sensitivity is the same as that of an intensity or incoherent interferometer.

If the receiver noise contributions are not negligible then the amplitude estimate from equation 9.32 will be biased since the squared fringe amplitudes are always positive. To calculate the magnitude of this bias consider the fringe visibility to be a vector of magnitude $\mathcal{A}$ oriented along the x axis to which a gaussian noise vector is added. The joint probability distribution of the x and y components of the resultant vector is

$$p(x, y) = \frac{1}{2\pi\sigma^2} e^{-\frac{(x-\mathcal{A})^2+y^2}{2\sigma^2}} . \tag{9.33}$$

It can be shown that the probability distribution of the magnitude of the visibility, $\mathrm{z} = \sqrt{x^2+y^2}$, is (e.g., Papoulos 1965)

$$p(\mathrm{z}) = \frac{\mathrm{z}}{\sigma} e^{-\frac{\mathrm{z}^2+\mathcal{A}^2}{2\sigma^2}} I_0\left(\frac{\mathrm{z}\mathcal{A}}{\sigma^2}\right), \ \mathrm{z} > 0 , \tag{9.34}$$

where I_0 is a modified Bessel function of zeroth order.

The expectation of z^2 can be calculated directly from equation 9.33 as the expectation of x^2+y^2. The result is $\langle z^2 \rangle = \mathcal{A}^2 + 2\sigma^2$. Hence in the presence of noise, equation 9.32 must be modified; an unbiased estimator of $\mathcal{A}$ is therefore

$$\mathcal{A}_e = \left[\frac{1}{N^2}\sum Z_i Z_i^* - 2\sigma^2\right]^{1/2} . \tag{9.35}$$

The procedure used more commonly than that of equations 9.32 or 9.35 to improve the sensitivity of an interferometric measurement is to segment the data into periods short with respect to the coherence time and average the squares of the fringe amplitudes. An unbiased estimate of the amplitude is

$$\mathcal{A}_e = \left[\frac{1}{N^2}\left(\sum z_i z_i^*\right) - 2\sigma^2\right]^{1/2} . \tag{9.36}$$

In the strong signal case where this form of coherent/incoherent averaging is not necessary, the signal-to-noise ratio improves as $N^{1/2}$, the same as for pure coherent averaging. In the low signal-to-noise ratio case, where incoherent averaging may be essential to improving the SNR or even detecting the fringes, the SNR only improves as $N^{1/4}$ for large values of N (Rogers, Doeleman and Moran 1995).

There is another statistical issue that should be addressed at this point. Often, it is necessary to search a large parameter space to find the signal or fringes. In the absence of signal the real and imaginary parts of the fringe visibility are zero-mean gaussian random variables and the magnitude, z, is a random variable with a Rayleigh distribution, as given by equation 9.34 for $\mathcal{A} = 0$ (Note that $I(0) = 1$). The probability distribution of the maximum of N samples, z_m, has a distribution that becomes progressively more biased as N increases. The mean value of z_m is about $\sigma\sqrt{2\ln N}$ for large N with an rms deviation of about $0.8\sigma\sqrt{\ln N}$. Hence, if one searched a two dimensional fringe rate/delay range of 10^6 points for a signal, the expectation of the largest noise peak would be $5\sigma \pm 0.06\sigma$. Hence, any "detection" less than 6σ is clearly suspect. Similarly, projections of the data may lead to a bias. For example, a common option in spectral line VLBI is to plot the peak amplitude in the fringe rate spectrum as a function of frequency. If the fringe rate spectra have N points then there will be a biased baseline in the frequency spectrum of $\sigma\sqrt{2\ln N}$. Note that for strong spectral line sources, σ is a function of frequency, and gives rises to the phenomena of "pseudo fringes".

It is important to be able to estimate the coherence time of an interferometer. This can be done empirically by subdividing the observation period into shorter and shorter segments and estimating the amplitude from equation 9.36. At some point when the phase fluctuations become small, the estimated fringe amplitude will reach its maximum and true value. The phase fluctuations that limit the coherent integration time are determined primarily by the atmosphere, but in some cases by the frequency standards. For an integration time T, the measured fringe amplitude will be given by

$$\mathcal{A}_m = \mathcal{A}\left|\frac{1}{T}\int_0^T e^{i\phi(t)}dt\right| = \mathcal{A}C(T)\ , \tag{9.37}$$

where $C(T)$ is a sample of the coherence function and ϕ is a sample function of the fringe phase the same as in equation 9.30. $C(T)$ is always less than or equal to unity and only if the phase noise is zero is $C(T) = 1$. Frequency standards are usually characterized by a quantity called the Allan standard deviation which describes the fractional frequency deviations of a sinusoidal waveform with phase noise. The Allan standard deviation has a precise statistical definition and it was invented to avoid problems with low frequency divergences in power spectra and to confound students. Examples of the Allan standard deviation are shown in figure 9.8. The Allan standard deviation, σ_y, is approximately the rms deviation in frequency divided by the frequency, $\Delta\nu/\nu_0$, or $\sigma_\phi/(2\pi\nu_0 T)$. Hence the coherent integration time, T_c, is approximately defined as the time for which the rms phase deviation is 1 rad,

$$2\pi\nu_0 T_c\sigma_y \cong 1\ . \tag{9.38}$$

A more precise connection between the Allan standard deviation and the coherence function for the case of white phase noise is given by (see Rogers and Moran

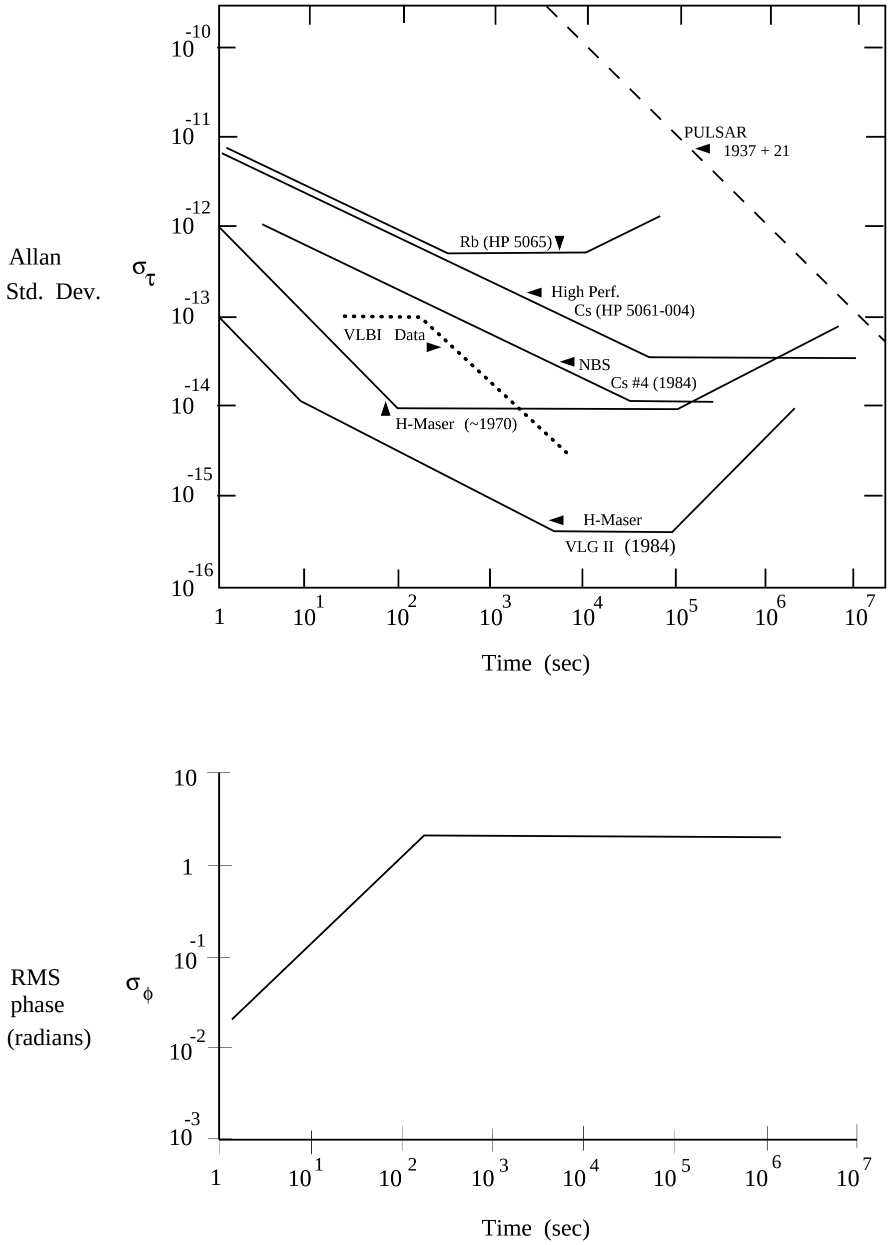

Figure 9.8: *Top:* Idealized plot of the stability of atomic frequency standards, the pulsar 1937+21 and actual VLBI data (from TMS). *Bottom:* The rms phase versus integration period for VLBI data at 22 GHz derived from the Allan standard deviation in the upper plot with the formula $\sigma_\phi \simeq \sigma_y \nu_o T$.

Table 9.2: Coherence times for $\sigma_y = 10^{-13}$

ν (GHz)	$T_c\,(\beta = 0.8)$ (s)	$T_c\,(\beta = 0.5)$ (s)
1	1840	3250
5	370	650
10	185	325
22	85	150
40	45	80
100	20	32
200	10	15

1981, or TMS)

$$\left\langle C^2\left(T\right)\right\rangle^{1/2} = e^{-\dfrac{2\pi^2\nu_0^2\sigma_y^2T^2}{3}} . \tag{9.39}$$

A more general definition of coherence time, the time for the $\langle C\left(T\right)\rangle^{1/2}$ to drop to β, is, from equation 9.39 ,

$$T_c = \frac{\sqrt{-6\ln\beta}}{2\pi\nu_0\sigma_y} . \tag{9.40}$$

Typical Allan standard deviations as a function of time for the atmosphere and frequency standards are shown in figure 9.8 (lapelled "VLBI data"). Note that the Allan variances are additive, so for VLBI application where two frequency standards are involved, the Allan standard deviation will increase by $\sqrt{2}$. A representative value is $\sigma_y \sim 10^{-13}$. The coherence times for $\beta = 0.8$ for various frequencies are given in table 9.2. For frequencies below about 1 GHz, the coherence time may also be affected by the ionosphere.

9.6.1 Atmospheric Effects on Phase and Delay

The atmosphere has a smooth component, which causes a systematic variation of delay in an interferometer, and a fluctuating component, causing short term phase noise. Consider first a short baseline interferometer under a homogeneous plane-parallel atmosphere of index of refraction n_0. The relation between the zenith angle of radiation impinging on the atmosphere at angle z and the observed angle z_0 is given by Snell's Law, $n_0 \sin z_0 = \sin z$. The interferometer delay is

$$\tau_g = \frac{b\sin z_0}{\left(\frac{c}{n_0}\right)} = \frac{b\sin z}{c} , \tag{9.41}$$

where c is the speed of light and b is the baseline length. Thus the atmosphere can be ignored in this simple approximation as long as the free space values for the speed of light and zenith angle are used in computing the delay. However, refraction must still be taken into account in pointing the telescopes in the direction of the source since the refractive angle correction is approximately equal to $\tan z$ in units of arc minutes!

The index of refraction profiles above the antennas in a VLBI array are different and the zenith angles are also different. It is best to consider the geometric delay for each antenna separately. In the zenith direction the atmosphere will introduce an excess propagation path of $L_0 = \int (n-1)\, d\ell$, where n is the index of refraction along the line of sight. Since n deviates from unity only by about 300 parts per million, it is usually described in terms of refractivity, $N = (n-1)\, 10^6$. For air the refractivity is approximately given by the two term Smith-Weintraub formula,

$$N \simeq \frac{77.6}{T}\left(P + 4810\frac{p_v}{T}\right), \tag{9.42}$$

where P is the total pressure in mbars, p_v is the partial pressure of water vapor in mbars and T is the temperature. The two terms on the right side of the equation are called the dry and the wet parts. The wet part is quite variable and typically has a scale height of about 2 km and the dry part can be estimated from the surface pressure and has a scale height of about 8 km. equation 9.42 is accurate to a few percent from DC to 1000 GHz at frequencies where the atmosphere is reasonably transparent. Hence the atmosphere introduces a frequency independent (i.e., non-dispersive) delay. A widely held misconception is that phase fluctuations are worse near the 22 GHz water vapor transition. This is not true. Equation 9.42 can be integrated along a vertical path to yield

$$L_0 \simeq 0.228P + 6.3w \;[\mathrm{cm}], \tag{9.43}$$

where w is the column height of precipitable water in cm. The first term contributes 231 cm for a standard pressure of 1013 mb and the second term varies from 0.6 cm during the best observing weather on Mauna Kea (17% of the time), to 30 cm in places like New Guinea.

Since the atmospheric opacity at radio frequencies is largely due to water vapor, it has long been hoped that the propagation delay could be estimated from measurements of sky brightness. For example at 22 GHz the atmospheric brightness temperature is about 13 w K. Hence a 10° shift of phase is caused by $\Delta w = 0.006$ cm, which causes a change in sky brightness of 0.08 K, which is a power change of 8×10^{-4} with a system temperature of 100K. At 230 GHz in an atmospheric window the brightness temperature is about 140 w and only 0.0006 cm of water vapor is needed to cause a phase shift of 10° and a brightness temperature change of 0.08K. Radiometry at 1.3 cm has been extensively developed to correct the interferometric delay for geodetic and astrometric VLBI, but with limited success. Technical problems include difficulty with precise calibration, the lack of validity in the algorithm under non-clear weather conditions and the difference in volume sampled by the near fields of the VLBI antenna and the small radiometer antenna. For this reason the zenith delay is normally estimated from the delay residuals in the interferometric data.

The excess path length at any zenith angle can be described in terms of the zenith excess path and a mapping function $m(z)$. Various mapping functions are

$$m_1(z) = \sec z \tag{9.44}$$

$$m_2(z) = \sec z - \frac{h_0}{r_0} \sec z \tan^2 z \tag{9.45}$$

and

$$m_3(z) = \cfrac{1}{\cos z + \cfrac{A}{\cot z + \cfrac{B}{\cos z + C}}} . \tag{9.46}$$

Model 1 is a simple plane-parallel atmosphere; model 2 is a Taylor expansion for a round earth of radius r_0 and exponential scale height h_0; model 3 (also known as CfA-2.2) which has free parameters A, B and C, is preferred by the geodetic VLBI community (Davis et al. 1985). The atmosphere can easily cause excess delays of 200 cm and fringe rates of several hundred mHz (at 22 GHz). Those effects are large and are generally removed by a delay model in the correlator. The observer is left to deal with residual errors and the effects of rapid fluctuations.

The rapid random component of atmosphere-induced phase noise is more difficult to deal with. The atmosphere can be characterized as a layer containing irregularities over a wide variety of scale sizes distributed according to the Kolmogorov model of turbulence. A plane wavefront impinging on this layer will have an emerging phase front at the ground given by $\phi(x)$, where ϕ is a gaussian random variable. (See figure 9.9). The observed visibility is

$$V = S e^{i(\phi_1 - \phi_2)} , \tag{9.47}$$

where the exponential function is just the $G_i G_j^*$ term of equation 9.1. The fluctuations are often characterized by the structure function of phase, given by

$$D_\phi(b) = \left\langle \left[\phi_1(x) - \phi_2(x-b)\right]^2 \right\rangle . \tag{9.48}$$

The structure function is of direct interest in interferometry because it describes the variance of the phase difference at the two antennas, which is precisely the quantity an interferometer is sensitive to (see equation 9.47). The relation between the structure function and power spectrum of the phase fluctuations, $P_\phi(q)$, is

$$D_\phi(b) = 4\pi \int \left[1 - J_0(qb)\right] P_\phi(q)\, q\, dq , \tag{9.49}$$

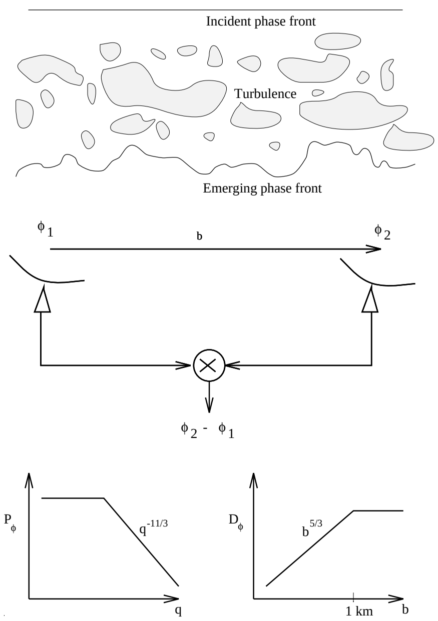

Figure 9.9: *Top:* A depiction of the effect of a turbulent medium on the phase of an incident wavefront. Note that unlike interstellar scattering, amplitude fluctuations are unimportant because the antennas are directly adjacent to the turbulent medium. *Bottom:* Spectrum and structure function of the phase fluctuations.

where J_0 is a Bessel function of order zero, and q is the spatial wavenumber. Hence, by use of equation 9.18, the ensemble average of the visibility in equation 9.47 is

$$\langle V \rangle = Se^{-D_\phi(b)/2} . \tag{9.50}$$

The structure function of the atmosphere is proportional to $b^{5/3}$ for distances up to a few kilometers. After that, atmospheric fluctuations on reasonable time scales are uncorrelated and D_ϕ becomes a constant. The rms phase noise on an interferometer is equal to $\sqrt{D_\phi(b)}$ and for short baseline interferometers is almost proportional to baseline length $\left(\sigma_\phi \sim b^{5/6}\right)$. For VLBI it becomes independent of baseline length.

9.7 Phased Arrays as VLBI Elements

When sensitivity is important it is advantageous to use all the available antennas at a location as a phased array element in a VLBI Network. Examples of arrays that have been used in this fashion are the VLA, OVRO, BIMA, and Westerbork. The undetected signals are summed after correcting for geometric delay and phase. The phased array forms a beam with an angular width of approximately λ/d_a where d_a is the size of the array. In the case of the VLA in the A configuration at 22 GHz the beam size is about $0.''1$. The position of the program source must be known to a small fraction of this size. It is often difficult to maintain adequate phasing of the array because of phase drifts in the array electronics and atmospheric turbulence. For large arrays, such as the VLA (A configuration), the coherence time due to atmospheric effects is about the same as for the VLBI array. The normal procedure is to phase the array on a calibrator source nearby in angle to the program source. Instrumental phases can be derived and the results applied to the received signals before summation (at the VLA the solutions from ANTSOL are used to adjust the phases in the array). The array will slowly dephase with time until the calibrator must be reobserved and the phases readjusted. If the program source is strong and compact, the array can be continually phased on it, so that decorrelation problems are avoided.

The sensitivity of a phased array can be calculated by the usual radiometric analysis. We can analyze the phased array and use the results in the normal way to calculate the SNR on a VLBI baseline. Suppose there are N identical elements in a phased array, i.e., equal system temperatures and antenna temperatures, T_S and T_A, respectively. The output of the summing port is

$$V(t) = \sum s_i(t) + n_i(t) \ , \tag{9.51}$$

where s_i and n_i represent the random signal and noise voltages from the ith element of the array, respectively, and $\langle s_i \rangle = \langle n_i \rangle = 0$ and $\langle s_i^2 \rangle = T_A$ and $\langle n_i^2 \rangle = T_S$. The power, obtained from the square of equation 9.51, is

$$\langle V^2 \rangle = \sum_{i,j} [\langle s_i s_j \rangle + \langle s_i n_j \rangle + \langle s_j n_i \rangle + \langle n_i n_j \rangle] \, . \tag{9.52}$$

If the array is perfectly phased, then $s_i = s_j$ and $\langle s_i s_j \rangle = T_A$, whereas if it is unphased, $\langle s_i s_j \rangle = T_A$ for $i = j$ and zero for $i \neq j$. Since $\langle s_i n_i \rangle = 0$, and $\langle n_i n_j \rangle = T_S$ for $i = j$ and zero for $i \neq j$, equation 9.52 can be reduced to

$$\langle V^2 \rangle = N^2 T_A + N T_S \text{ (phased)} \tag{9.53}$$

$$= N T_A + N T_S \text{ (unphased)} \, . \tag{9.54}$$

To calculate the noise level we first need to calculate $\langle V^4 \rangle$, which (from the fourth-order moment theorem for gaussian random variables) is approximately $3N^2 T_S^2$ for $T_S \gg N T_A$. Hence the rms fluctuation level in power is given by $\left[\langle V^4 \rangle - \langle V^2 \rangle^2\right]^{1/2} \cong \sqrt{2} N T_S$. Since there are $2\Delta\nu T$ independent samples averaged in integration period T, the SNR is given by

$$SNR = \frac{N T_A}{T_S} \sqrt{\Delta\nu T} \text{ (phased)} \tag{9.55}$$

$$= \frac{T_A}{T_S} \sqrt{\Delta\nu T} \text{ (unphased)} \, . \tag{9.56}$$

Hence the array functions as an element with a collecting area equal to the total area of the array when it is phased properly and with the collecting area of a single element when it is randomly phased. Note that if the phased array were used for radiometry (and not for interferometry) then one might consider averaging the detected signals (i.e., power) from each antenna. In this case the phasing doesn't matter and the SNR is

$$SNR = \sqrt{N}\frac{T_A}{T_S}\sqrt{\Delta\nu T}\,, \tag{9.57}$$

which is intermediate between the two cases given in equations 9.55 and 9.56.

If the atmospheric conditions are marginal, then care must be taken to make effective use of a phased array. For example, with the VLA the antennas are spaced in distance from the array center according to a power law with exponent 1.72. Since the atmospheric phase noise increases approximately linearly with distance, as described in section 9.6.1, the phase noise on the outer three antennas will be about twice that of any of the other antennas. Suppose we had the situation where the phase noise was acceptable on the seven inner antennas on each arm but effectively random for the outer two antennas. Dropping the outer 6 and retaining the inner 21 would increase the SNR of the array by 25% and increase the SNR of a VLBI baseline formed with the phased array by 12.5%.

Another problem with phased arrays such as the VLA is that the performance among antennas can vary widely. If the receiver temperatures are different, the receiver voltages should be weighted in proportion to T_{si} to obtain optimum results. However, at the VLA the signals are quantized before summation so the weighting is effectively $(T_{si})^{1/2}$. The SNR ratio is less than optimum by the factor

$$F = \frac{\left(\sum \frac{1}{\sqrt{a_i}}\right)^2}{N\sum \frac{1}{a_i}}\,, \tag{9.58}$$

where $a_i = T_{s_i}$. For an rms variation in performance among the antennas of 20%, F is about 0.9. However, it is advantageous to remove very poorly performing antennas from the array. Decision strategies on which antennas to include when an array is being upgraded are discussed by Moran (1989). In the more general case where both the receiver temperatures and the antenna gains vary, the optimum weighting is $T_{s_i}/\sqrt{T_{A_i}}$ (Dewey 1994). This result may seem strange, but it is entirely consistent with the well-known concept that the optimum sensitivity in interferometric imaging is achieved by weighting the visibilities in Jy by the product of the SEFDs of the elements (see also Rogers 1991).

9.8 The Impact of Calibration Errors in Images

In spite of one's best efforts, there will always be residual calibration errors. One can always get an idea about how well the calibration has succeeded by checking the corrected visibilities at crossing points in the (u, v) plane. Since VLBI arrays rarely have exactly EW baselines, the (u, v) tracks on different baselines will occasionally cross providing an opportunity for this check.

We concentrate here on the effect of multiplicative errors (see Ekers 1989) of the form

$$V'(u, v) = V(u, v)\, G(u, v) \ , \tag{9.59}$$

where $G(u, v)$ is the residual complex gain, now referred to a point in the (u, v) plane. It may or may not be factorable into station dependent components. These gain factors are what is left over after calibration has been applied. Since $G(u, v) = G^*(-u, -v)$, i.e., it is a Hermitian function, the magnitude of the gain error is an even or symmetric function of u, v and the phase is an odd or antisymmetric function. Consider first the amplitude errors in one dimension. As depicted in figure 9.10, multiplicative amplitude errors can be represented as a convolution in the image plane. Hence, a uniformly weighted map with no amplitude errors would give a sinc function dirty beam (or a $J_1(2\pi u_m \theta)/(\pi u_m \theta)$ Bessel function in two dimensions). Suppose one measurement out of a total of N has a gain error that is off by a factor of 2. Because of the linearity of the Fourier transform, the dirty beam will be the expected one, plus an additional sinusoidal component. Hence the dirty map of a compact source will be the normal convolved image plus stripes with period $1/u_0$, where u_0 is the spacing of the offending data point in the (u, v) plane. In general, the amplitude errors will have some complicated distribution, which will result in a symmetric dirty beam, since the Fourier transform for a real symmetric function is also real and symmetric. If the characteristic scales for variation in the amplitude variations is Δu_c, then the extent of the dirty beam will be $1/\Delta u_c$.

In two dimensions the NS coverage is rarely as good as the EW coverage. Hence the dirty beam is elongated in the NS direction. The axial ratio gets larger as the declination of the source decreases. For a source near the equator this axial ratio might be 5:1. The tracks will be more closely spaced in v than u. Hence the characteristic scale for changes in v will be smaller than for u, Δv and Δu respectively. Hence, the extent of the error beam will be Δu^{-1} and Δv^{-1} in the x and y directions of the image. In other words, amplitude errors lead to symmetric artifacts in the image that tend to be extended preferentially along the major axis of the dirty beam. Another way to understand this result is as follows. The v axis in the (u, v) plane can be stretched to make the coverage in both dimensions the same. The dirty beam in the modified coordinates (compressed x axis) will be nearly circularly symmetric (note however that circularly symmetric sources will now appear elongated). Clearly, fringe amplitude errors will give rise to artifacts which are distributed in a circularly symmetric fashion in a statistical sense. Now, when the x axis is stretched to its normal value in the image plane, the beam and the artifact distribution will be elongated in the same direction. (In the early days of interferometry some astronomers published images in coordinates that made the beam circular. This presentation was good for judging the error

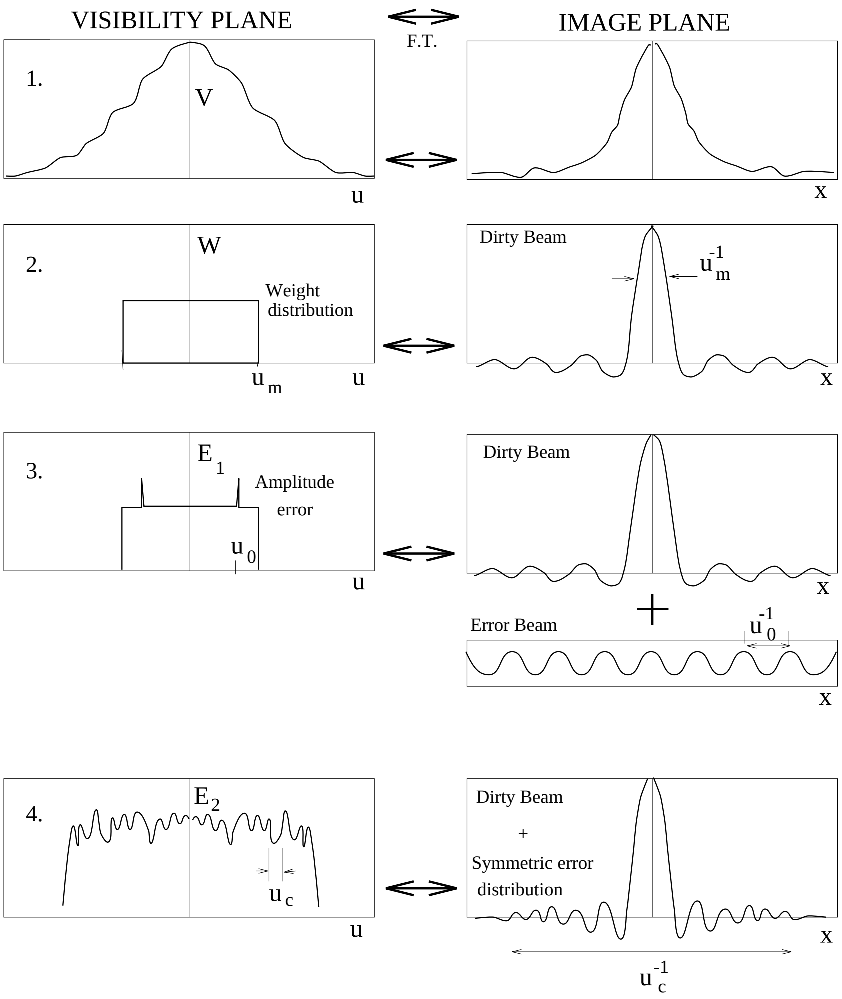

Figure 9.10: The effect of amplitude calibration errors on the interferometric image. *From the top: (1)* The true source visibility and its Fourier transform, the image; (2) The weighting function describing the (u, v) plane coverage and its transform, the dirty beam; (3) The weighting function with a single calibration error and its transform; (4) The weighting function for a random distribution of errors, and its transform.

artifacts, but not so good for interpreting the source structure.)

Phase errors give rise to antisymmetric artifacts, and like amplitude errors can scatter the energy of a point source over the field of an image. In one dimension the image is

$$I(x) = \frac{1}{N} \sum V_m e^{i2\pi ux} e^{i\phi(u)} , \tag{9.60}$$

where $\phi(u)$ is a gaussian random variable. If the source is unresolved and has a flux density S, then $\langle I(0) \rangle = Se^{-\sigma^2/2}$ and the strength is reduced by the phase noise. In principle, the total flux can be recovered through application of Parseval's theorem

$$\sum I^2(x) = \frac{1}{N} \sum V_m^2 = S^2 , \tag{9.61}$$

but this relation is of little practical use and subject to the normal noise bias problem described in section 9.6.

A common practice in VLBI processing is to apply the phase closure condition in hybrid mapping (or self-calibration) and not the amplitude closure condition. This is because no mapping can generally be done at all without the use of phase closure. Application of the amplitude closure sometimes causes instability in the self-calibration because of the larger fraction of information that must be supplied. Hence, the most insidious type of errors are the amplitude errors, which can lead to symmetric "jet/counterjet" artifacts.

9.9 Summary

Here are a few things to remember about calibration.

1. The complex gain factors relating the measured and true visibility are either baseline or station dependent. Station dependent errors are removed in the process of self-calibration, which makes use of phase and amplitude closure relations. Self-calibration does not fully supply the calibration information for a small array and it also requires high SNR for implementation. Astrometry requires precise calibration of delay and/or fringe rate data.

2. Amplitude calibration requires measurement of the receiver temperature, atmospheric opacity and antenna gain curve. The first two quantities can be obtained from tipping scans (in reasonable weather conditions) and the last by measuring the antenna temperature of a source as a function of zenith angle. Pointing errors and polarization mismatch cause additional amplitude calibration errors, which are hard to measure.

3. Where the SNR is low, estimates of fringe amplitude will be biased. Searching for fringes often involves probing a large parameter space; watch out for large noise bumps.

4. Phase calibration is not usually possible. Primary consideration is given to dealing with phase noise as introduced by the frequency standards and atmosphere. The atmosphere is essentially non-dispersive at radio frequencies and the phase noise (in turns) for a sea level network at temperate latitudes is approximately given by $10^{-13}\nu T$ where ν is the frequency in Hz and T is the integration time in sec. To integrate longer you must segment the data or use Parseval's theorem on the fringe rate spectrum.

5. A phased array can be used as an element in a VLBI array. However, the coherence time for a phased array (e.g., VLA/A) may be about the same as for the VLBI array. The effective area of the phased array of N antennas will vary from that of a single antenna to that of N antennas depending on the quality of the phasing. In the case of the VLA/A at 22 GHz, the beam of the phased array is rather small, about 0.1 arcsec, and the source position must be known to better than this accuracy beforehand.

6. Residual amplitude errors in the data lead to symmetric artifacts in the data whose distribution is elongated and oriented in the same direction as the dirty beam. Residual phase errors yield antisymmetric artifacts.

We are grateful to J. R. Herrnstein, M. J. Reid, Z. Q. Shen, and A. R. Thompson for helpful comments.

References

Clark, B. G. 1968. "Radio interferometers of an intermediate type". *IEEE Trans. Ant. Prop.* **AP-16**, 143.

Davis, J. L., Herring, T. A., Shapiro, I. I., Rogers, A. E. E., & Elgered, G. 1985. "Geodesy by radio interferometry: effects of atmospheric modelling errors on estimates of baseline length". *Radio Sci.* **20**, 1593.

Dewey, R. J. 1994. "The effects of correlated noise in phased-array observations of radio sources". *Astron. J.* **108**, 337.

Ekers, R. D. 1989. "Error recognition". In R. A. Perley, F. R. Schwab, and A. H. Bridle (Eds.), *Synthesis Imaging in Radio Astronomy.* San Francisco: Astronomical Society of the Pacific, p. 199.

Leppänen, K. J. 1993. "Opacity correction for high frequency VLBI observations". VLBA Scientific Memorandum 1, National Radio Astronomy Observatory, Socorro.

Lo, K. Y., Backer, D. C., Kellermann, K. I., Reid, M., Zhao, J. H., Goss, W. M., & Moran, J. M. 1993. "High-resolution VLBA imaging of the radio source Sgr A* at the Galactic centre". *Nature* **362**, 38.

Moran, J. M. 1989. "Introduction to VLBI". In M. Felli and R. Spencer (Eds.), *Very Long Baseline Interferometry.* Volume 283 of *NATO ASI Series C.* Dordrecht: Kluwer, p. 27.

Papoulis, A. 1965. *Random Variables and Stochastic Process.* New York: McGraw Hill.

Pearson, T. J., & Readhead, A. C. S. 1984. "Image formation by self-calibration in radio astronomy". *Ann. Rev. Astron. Astrophys.* **22**, 97.

Rogers, A. E. E. 1991. "Very long baseline interferometry fringe detection thresholds for single baselines and arrays". In H. Hirabayashi, M. Inoue, and H. Kobayashi (Eds.), *Frontiers of VLBI.* Tokyo: Universal Academy Press, Inc., p. 341.

Rogers, A. E. E. 1993. "Advances in VLBI techniques". In W. R. Stone (Ed.), *Review of Radio Science 1990–1992*. Oxford: Oxford University Press, p. 657.

Rogers, A. E. E., Doeleman, S. S., & Moran, J. M. 1995. "Fringe detection methods for very long baseline arrays". *Astron. J.* **109**, 1391.

Rogers, A. E. E., & Moran, J. M. 1981. "Coherence limits for very long baseline interferometry". *IEEE Trans. Inst. Meas.* **IM-30**, 283.

Rolfs, K. 1986. *Tools of Radio Astronomy*. Heidelberg: Springer.

Thompson, A. R., Moran, J. M., & Swenson, G. W., Jr. 1986. *Interferometry and Synthesis in Radio Astronomy*. New York: Wiley-Interscience. First (1991) and second (1994) reprintings by Krieger Pub. Co., Malabar (Florida).